Numerical and Experimental Resource Assessment for a Tidal Turbine in the Tagus River Estuary

B. Hoofd, T. Gomes, L. Pinto, G. Vaz, R. Neves, A. Botelho, and C. Freitas

Abstract—**Lisbon, the capital of Portugal, is located on the mouth of the Tagus River, where the current speed and direction are mainly governed by the local tides. The narrowest part of the river is located between Lisbon downtown and the western side of the city. This narrowing accelerates the water flow and makes it a potential site for a tidal energy system. A preliminary study based on numerical simulations using the software MOHID was conducted to assess potential energy yields throughout the estuary using freely available hindcast data. This allowed the selection of three potential sites for a tidal turbine in the Lisbon area based on yearly tidal and current energy density: off the coasts of Cacilhas, Belém, and Paço de Arcos. However, even if the current model has been previously validated with experimental data, it was only done at two locations in the estuary that are far from the potential sites. Due to the complexity of the phenomena driving the current speed at these locations, additional validation is necessary before committing to a specific site. This paper presents the numerical analysis, the experimental campaign and the validation of the results at those three locations. Drifters with sails of 3.4m and 4.5m depth were released at least 8 times at each location and retrieved after 15 minutes of free drift. Each drifter was tracked with a GPS and the current speed and direction were derived from the drifters' trajectory. The analysis of the experimental data shows good agreement with the model, even though an error of 0.3m/s is consistent throughout the tests. This paper concludes with a discussion on the various parameters that could be the source of the differences between the numerical and experimental data.**

Index Terms—**MOHID, Tidal energy, Validation, Current drifters, Numerical Modelling, Tagus River, Experiments.**

I. Introduction

WIND and solar photovoltaic are the most harvested resources of renewable energy [1] used across the world to decrease local carbon footprint while answering the energy needs. However, the technologies to harvest large amount of solar and wind energy are usually not well suited for an urban environment because they require large surface areas and undisturbed resources, which is not possible at the vicinity of high buildings that both distorts the wind flow and shades the solar panels. On the other hand, cities built at an estuary can benefit from the combined power of the river current and of the tides using hydrokinetic turbines to harvest their energy. In the case of Lisbon, the tides are the dominant factor of the current speed [2], which means that seasonality and extreme weather events would have only limited impact on the power production, hence facilitating the management of the power input to the grid.

Existing studies can provide insights on the current speed distribution in the Tagus estuary. For example two experimental campaigns, [3] and [4], were conducted to assess the current velocities at more than 10 locations in the Tagus River. They used Acoustic Doppler Current Profilers (ADCP) installed at various depths below the water level. In both studies, only the partial analysis of the data can be found, and not the raw data. The authors showed nonetheless a clear acceleration of the flow around the 25 de Abril bridge based on the measurement from the Autoridade do Porto de Lisboa in 1987, and a great variability across the estuary using data collected by the Faculty of Science of the University of Lisbon between 1985 and 1989. In both cases, the measured velocity peak is approximately 1.5m/s. However, those measurements are more that 30 years old, and climate change or dredging activities might have significantly altered the dynamics of the estuary. It is therefore crucial to conduct new numerical and experimental campaigns.

The numerical tool MOHID [5] was specifically designed to study such complex hydrodynamic behaviour of coastal areas. It is an open-source tool that is continuously improved and updated by the MOHID community. Originally developed by the Marine and Environmnetal Technology Research Center (MARETEC), it started as a bi-dimensional hydrodynamic model [6], and was later updated for a three-dimensional (3D) version including 3D lagrangian and 3D eulerian transport models [7]. The tool allows the adoption of an integrated modelling philosophy, not only of processes - physical and biogeochemical -, but also of different scales - allowing the use of nested models - and of systems - estuaries and watersheds -, due to the adoption of an object oriented programming philosophy. MOHID was validated against experimental data in [8] and [9] using the Tagus estuary as a test case, but the validation was conducted only on a limited amount of locations. MARETEC has an operational model based on MOHID for the Tagus estuary that

B. Hoofd, T. Gomes and G. Vaz are with blueOASIS, EBF, R. Prudêncio Franco da Trindade 4, 2655-344 Ericeira, Portugal (e-mail: info@blueoasis.pt).

L. Pinto and R. Neves are with MARETEC/LARSyS, Instituto Superior Técnico, Universidade de Lisboa, Av. Rovisco Pais 1, 1049-001 Lisboa, Portugal (email: ligia.pinto@tecnico.ulisboa.pt).

A. Botelho and C.Freitas are with the Municipality of Lisbon, Av. Dr. Francisco Luis Gomes, 1 Porta 3, Bloco 3.9 (Edifício Entreposto), 1800-177 Lisboa, Portugal (email: catarina.freitas@cm-lisboa.pt).

Digital Object Identifier:
https://doi.org/10.36688/ewtec-2023-258

offers hourly forecasts of multiple variables including water elevation, salinity, current speed and direction [10]. The spatial and temporal discretisation (1h and 200m) of this operational model is however not refined enough for a detailed analysis.

In this work, we first use this operational model to conduct a statistical analysis of the energy distribution in the Tagus estuary to highlight three potential sites for a tidal energy system to power Lisbon. This analysis also considers the availability of on-shore power stations at the vicinity of the sites, a parameter that has a significant impact on the levelized cost of energy. At each of these sites, an experimental campaign was conducted using GPS-tracked drifters to measure their drift and to deduce from this information the current speed. The experimental results were then compared to the outputs of the operational model to validate it. Both numerical and experimental analysis showed similar trends, despite variations in current intensities.

The paper is organised as follows: first the numerical analysis to select the three potential sites is presented. Then, the experimental setup using robust low-cost drifters is detailed, followed by the methodology for the data analysis. A comparison between the model results and the experiment is then proposed. Finally a discussion on the assumptions is described to explain the differences between the experimental and numerical results.

II. Preliminary numerical resource assessment

A. MOHID model

The core of the MOHID Water modelling system is a fully three-dimensional hydrodynamic model which solves the Navier-Stokes equations, considering the Boussinesq and hydrostatic approximations. The equations are numerically solved by using the Finite Volume method with a generic vertical discretization, which allows for the simultaneous implementation of various types of vertical coordinates.

The Tagus estuary model was implemented by using a downscaling approach, described by [11]. Three domains were nested in an online one-way approach to properly represent the tidal forcing at the ocean boundary. The first domain has a grid resolution of $0.06°$, covering the entire West Iberia coast ($33.5°N$ and $49.9°N$, $1.0°W$ and $13.5°W$) and was forced only with the FES2004 (Finite Element Solution) tidal atlas [12]. The second domain was used to smooth down the changes between the first and third domains grid resolution, minimizing numerical instabilities. With a grid resolution of $0.02°$, the second domain covers part of the Portuguese coast ($36.0°N$ and $39.9°N$, $8.5°W$ and $10.5°W$). The bathymetry of the first two domains generated from the ETOPO 20 database (http://www.ngdc.noaa.gov/mgg/global/etopo2.html). The last domain includes the Tagus estuary and part of the nearest coast ($38.5°N$ and $39.1°N$, $8.7°W$ and $9.6°W$) and has a variable resolution, with $0.002°$ (200 m) inside the estuary, and a time discretisation of one hour. The bathymetry was generated by using data collected during several bathymetric surveys, provided by the Portuguese Hydrographic Institute.

TABLE I
Sites location

Symbol	Location	Latitude	Longitude
L_1	Paço de Arcos	38.686807°	-9.292010°
L_2	Belém	38.691339°	-9.190508°
L_3	Cacilhas	38.688337°	-9.162385°

B. Selection of potential sites

The analysis was carried out on the Tagus estuary numerical model, as described in Section II A. The analysis was limited to points with a water depth above 3.4m, to avoid areas where the turbines would not fit underwater, and between the following latitude and longitude: $38.64°W$, $38.74°W$, $-9.35°N$, $-9.10°W$. For each remaining point of the grid, the modelled current velocity at each time step was analysed. The occurrence of instances having a current above 1m/s at each spatial point during a certain period of time was calculated as the ratio between the number of time instances with a current velocity above 1m/s and the total number of instances during that period of time. This analysis was done with two time scales: yearly and monthly. Figure 1 presents that percentage between September 2020 and September 2021 and the same percentage for the following year, between September 2021 and September 2022. Both years highlight two points of higher currents: East of the 25 de Abril Bridge, as presented in [3], and slightly west of the coast of Paço de Arcos. Figure 2 presents a similar analysis but for one month in each season. It seems to show that there is little seasonality and that the flow is mainly tide driven rather than river flow driven, as detailed in [2]. This analysis should however be repeated on multiples years to include high flow events occurring during ”wet” years, but those years were unfortunately not included in the Tagus estuary operational model, and this step was neglected.

Two potential sites were therefore clearly identified from their energetic point of view. However, one must also consider the distance to the electrical substations as a design parameter. Indeed, sub-sea power cables represent a significant cost both in terms of CapEx and OpEx [13]. Given the location of the substation in Belém, an additional site was identified off its coast. Finally, the presence of the navigation channel was also considered as a constraint: the turbine must not interfere with the navigation. This lead to the final three potential locations presented in Table I and Figure 3.

III. Experimental set up

A. Equipment

The flow measurements were done using simple drifters equipped with a GPS. Each drifter was composed of a self-made Styrofoam floater with a water

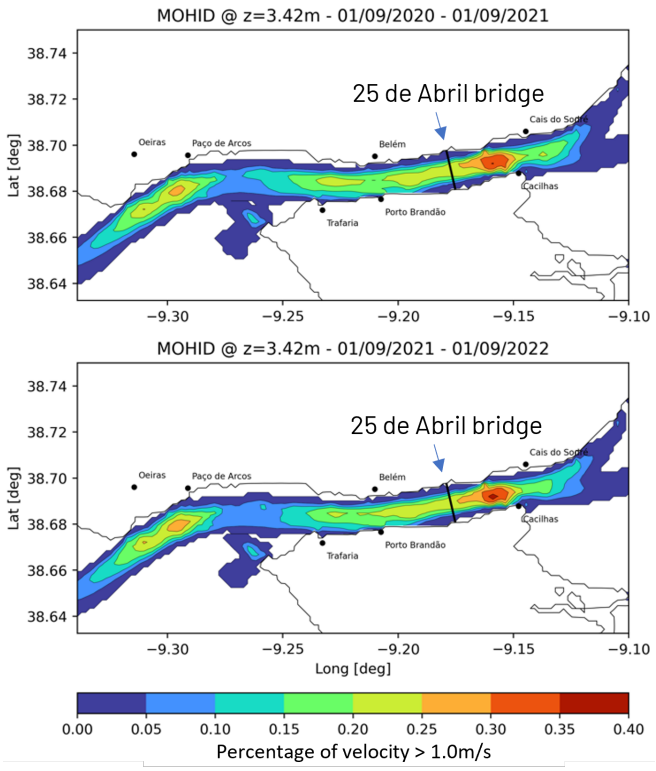

Fig. 1. Analysis of zones of higher current. Top: between 09/2020 and 09/2021. Bottom: between 09/2021 and 09/2022.

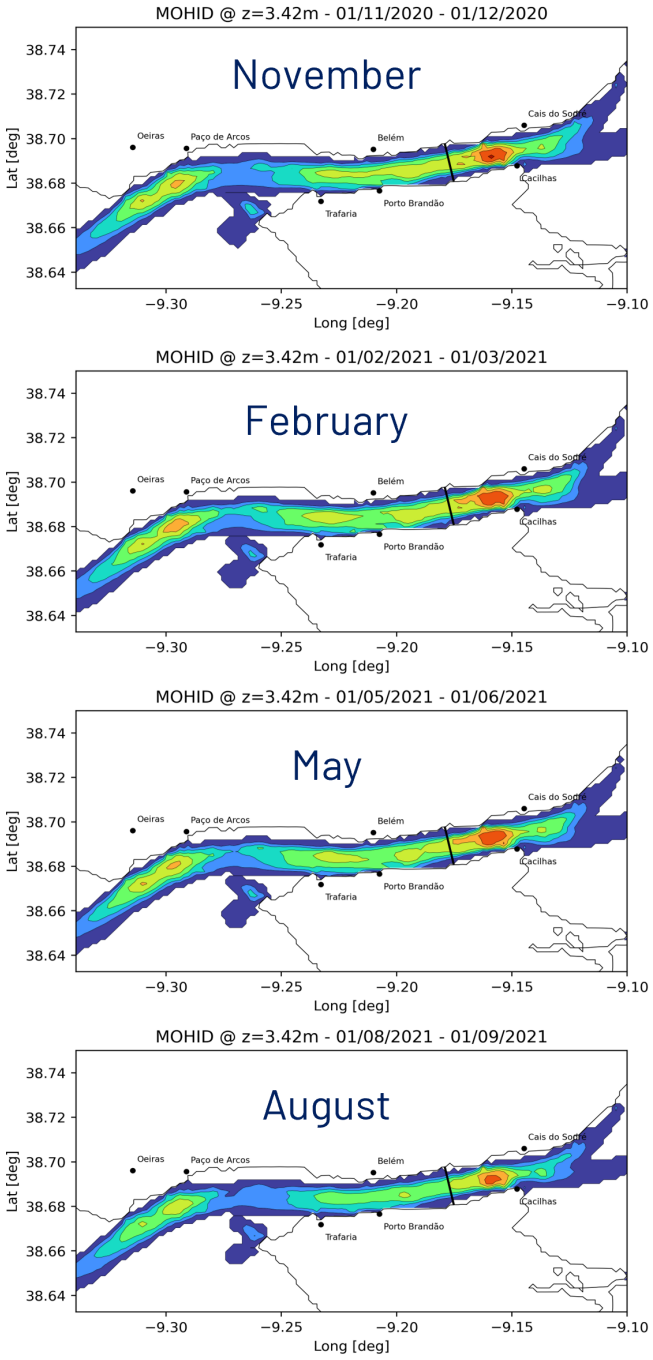

Fig. 2. Evolution of the current potential through the seasons. From top to bottom: Autumn, Winter, Spring, Summer.

casing where the GPS could be placed. The floater was then connected to a flexible steel wire, which allowed the adjustment of the depth of the sails. The sails were mounted as a cross on a steel frame using one vertical pole attached to the steel wire and four horizontal poles. The sails were made out of flexible, hard-to-puncture plastic sheets attached to the horizontal poles with small 3D-printed clips. Finally, a relatively heavy chain was placed at the bottom of the main pole to ensure that the drifters would remain vertical in the water. Pictures of the drifters, their dimensions and details of the connections are presented in Figure 4. In total, 4 drifters were built, with two different sails depths: 3.4m and 4.5m. The first depth corresponded to one of the discretisations of the numerical model, and the second depth corresponded to a more realistic rotor depth for a tidal energy device.

The GPSs used were the Sport LogBook GT-740FL-S, which have the advantages of being low-cost, small and water resistant. Its frequency of acquisition was set to the smallest available option: 1 second. Its accuracy in latitude and longitude was 10^{-6} degrees, which corresponds to an accuracy of 1m. Each GPS provided, for each point of measure, a time stamp, a latitude and a longitude coordinates.

A Rigid Inflatable Boat (RIB) (Figure 5) was used to release the drifters. The RIB was large enough to accommodate for the four drifters, two crew members to navigate the boat, and two crew members to conduct the tests.

B. Test protocol

The test protocol was defined as follows. Before sailing out, the crew turned on all GPSs and secured them in the water-tight compartments. The crew then sailed to one of the locations (L_1, L_2 or L_3) and released the four drifters, one by one, noting the time of each release. The drifters were left to drift for 15 min or until they drifted too close to a vessel sailing in the area. In both cases, the drifters were manually recovered thanks to the low free board of the RIB. The time of each recovery was carefully recorded. The test was then repeated four times at the same location. The crew would then sail to the other locations and reproduce the series of launch and recovery. All drifters were

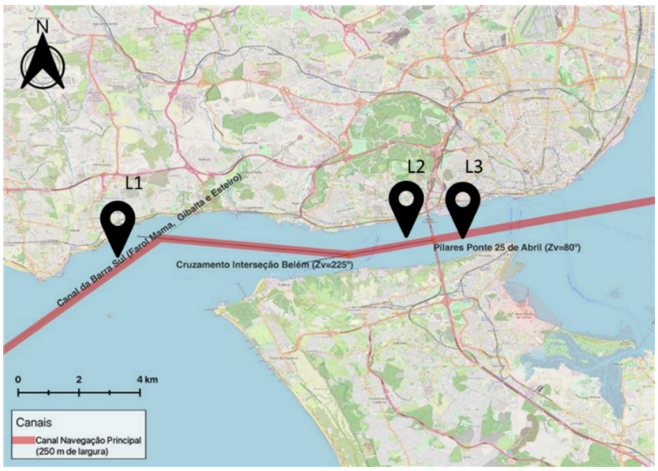

Fig. 3. Potential locations of tidal turbines in the Tagues River, the pink line representing the navigation channel.

Fig. 4. Drifter design. Top left: top view. Bottom left: bottom of the floater. Right: side view.

recovered after the experimental campaigns.
Two test days were chosen to capture the current speeds occurring at different moments in the tidal cycle: one day (D1) with a high tidal range (up to 3.1m) on the 23/11/2022 and one day (D2) with a low tidal range (down to 1.5m) on 01/02/2023. Figure 6 presents the expected current speeds for those two days at a 3.4m depth, as modelled by the operational forecast presented in Section II. As expected, the current velocities are much higher on D1 than on D2. In Figure 6, the times have been shifted to synchronise the high tides and facilitate the comparison.

IV. Analysis of the drifter speed

A. GPS and data processing

The GPS of each drifter was active throughout the days of testing. The first step of the analysis was therefore the selection of the time period corresponding to the actual drift using the GPS time stamps and the notes of the onboard crew regarding the times of

Fig. 5. RIB used for the test.

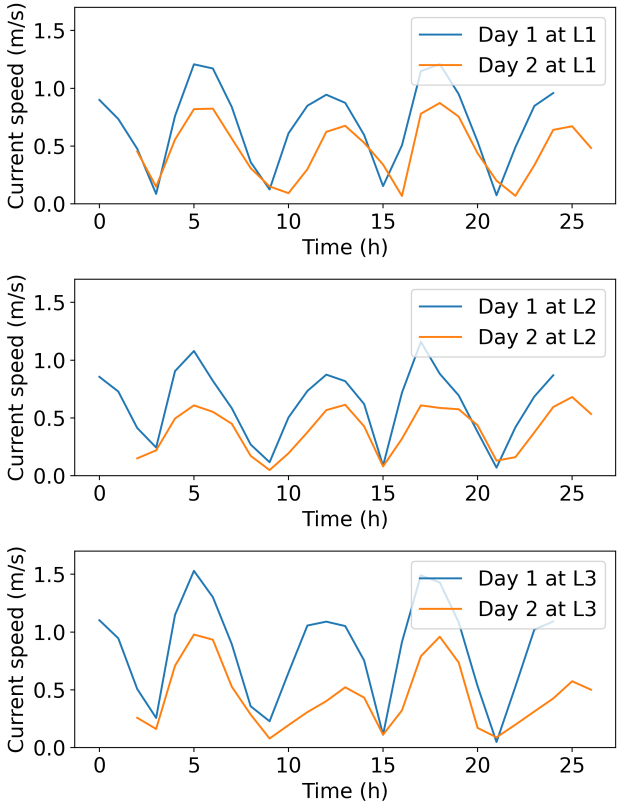

Fig. 6. Modelled variation of current speed in the two test days. Top: L1. Middle: L2. Bottom: L3.

release and recovery. Error points showing geographical coordinates outside of the region, as defined in Section II, Part B, were also removed. For the selected time segments, the distance between each data point was calculated from the coordinates using the Geopy python library [14], which calculates the shortest distance on the surface of the earth using the WGS-84 ellipsoid model. Given the relatively low accuracy of the GPS compared to the slow speed of the drifters,

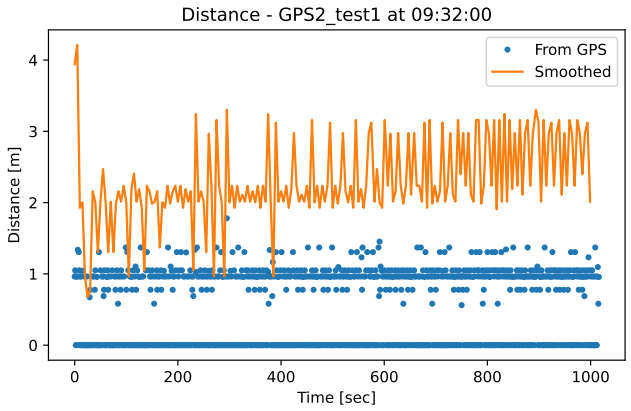

Fig. 7. Example of smoothing with a time window of 5 seconds.

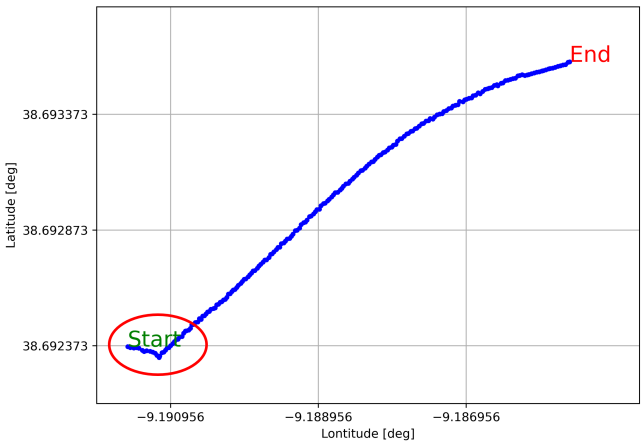

Fig. 8. Example of test window refinement using the trajectory of the drifter: circled time steps removed from the analysis.

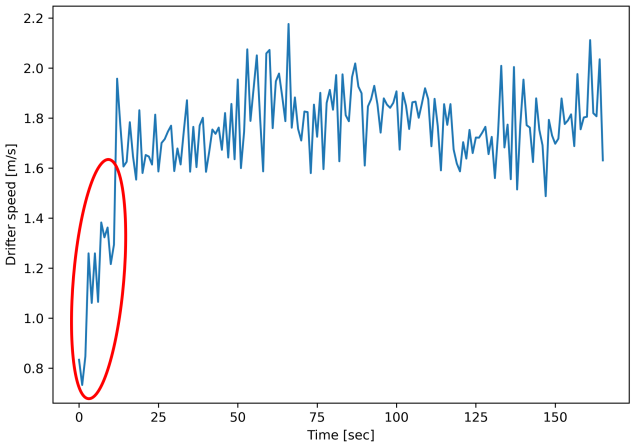

Fig. 9. Example of test window refinement using the speed of the drifter: circled time steps removed from the analysis.

this analysis gave a discrete signal with multiple measures of distance equal to 0m. To smooth the signal, a window of 5 seconds, i.e. 5 time steps, was used and the total distance travelled during those 5 seconds was considered for the next steps of the analysis. Figure 7 presents the difference between the initial and the smoothed signals. The speed was then calculated by dividing the measured distance by the window length. This was then repeated to derive the acceleration of the drifter from its speed.

The direction of the drift θ was calculated using trigonometry, first oriented to the east, as presented in Equation (1)

$$\theta = \arctan\left(\frac{(lon(t+w) - lon(t))}{(lat(t+w) - lat(t))}\right), \qquad (1)$$

where lon is the longitude, lat is the latitude, t is the time stamp and w is the width of the smoothing window. The direction is then translated to a Northward orientation, with degrees increasing clockwise, as per the usual reference system.

The time window for each test was then refined by analysing the drifters' trajectory and speed. If a sharp change of direction, as presented in Figure 8, and/or a sudden change of speed, as presented in Figure 9, was observed, it was assumed that the drifter was in fact on the boat and not drifting. Those points, highlighted by the red circles in both figures, were then removed from the analysis.

B. Drifters analysis

The drifters speeds and their trajectories for each test, each drifter and each location are presented in Figure 10. Due to the lower current speed in day 2, the trajectories are less straight and the velocities are lower. Figure 11 presents the average, minimum, maximum and standard deviation of the drifter speed for each release. This highlights the fact that in day 2, the standard deviations are higher than on day 1. This is explained by the relatively low accuracy of the GPS for very low speeds. Indeed, as described in Section III, the GPS accuracy is only 1m. Using a longer smoothing window would reduce the variability, but it was kept as 5 seconds for consistency and because a sensitivity analysis showed little impact of the smoothing window on the average speed for a test of 15min.

V. Validation of the Numerical Model

In this section we compare the current speeds as predicted by the Tagus estuary operational model (Figure 6) and the current speeds derived from the drifters' drifts.

A. Equation of motion of the drifters

The drifters' behaviour is mainly driven by the following forces [15]: gravity force (F_g) due to the drifter mass, the buoyancy force (F_b) due to its volume under water, the drag force from the wind (F_{Dw}), the drag force from the current (F_{Dc}), the force related to the added mass (F_{m_a}), the history force (F_{hist}), also called Basset or turbulence force that occurs due to the variability of the acceleration of the flow, and the pressure gradient force (F_p), related to the variation of pressure across the surface of the drifter. The equation of motion, in Lagrangian form, can therefore be written as such,

$$m\dot{v}_d = F_g + F_b + F_{Dw} + F_{Dc} + F_{hist} + F_{m_a} + F_p. \qquad (2)$$

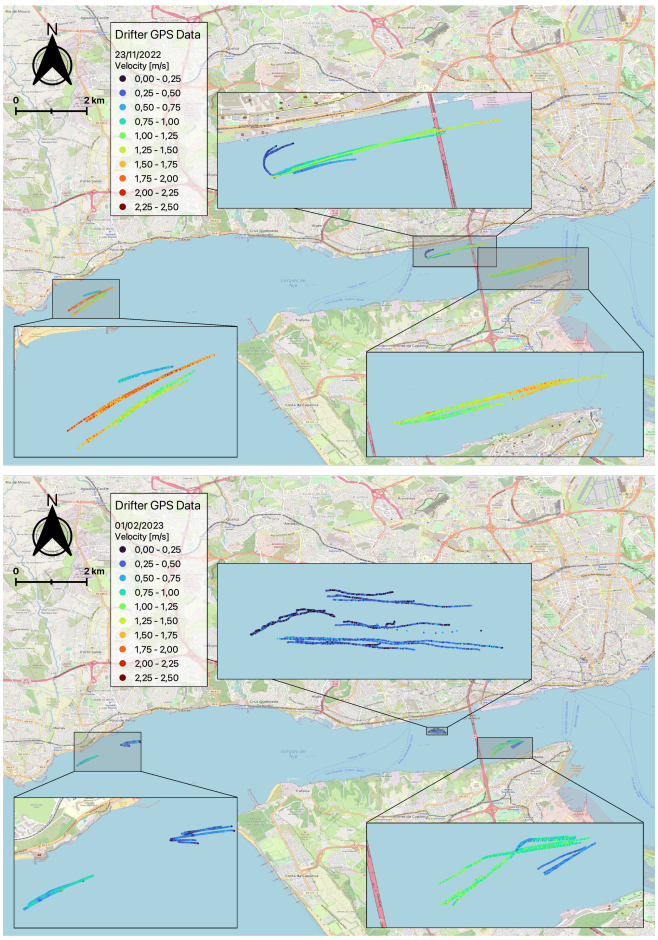

Fig. 10. Trajectory and speed of the drifters. Top: Day 1. Bottom: Day 2.

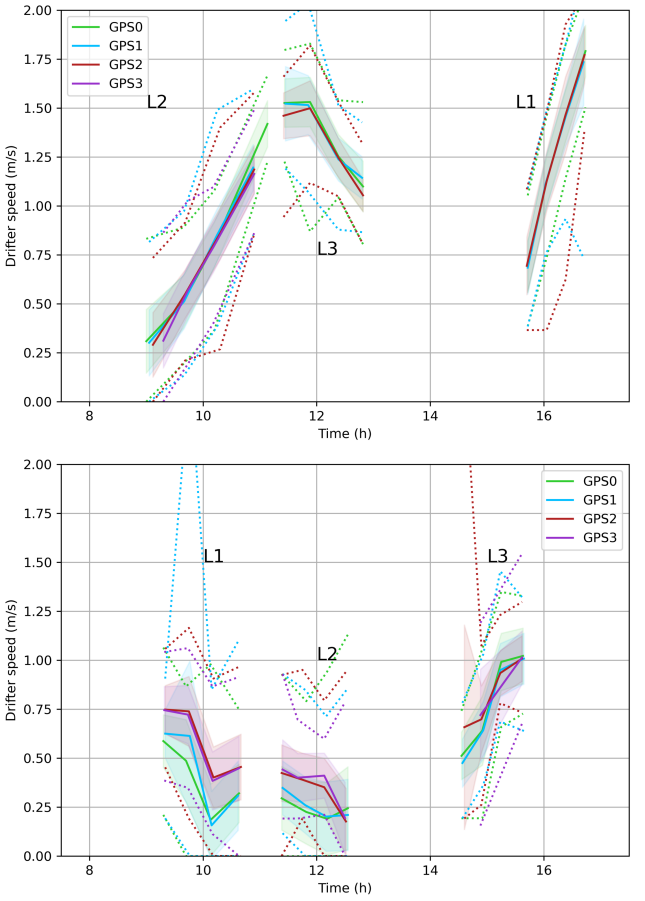

Fig. 11. Drifter speed during each test. Top: Day 1. Bottom: Day 2. Full line: average during a test. Colored section: with standard deviation. Dotted line: extrema.

Both F_b and F_g act on the vertical direction and balance each other out since the drifter is floating, and they are removed from the analysis.
The drag force can be quantified based on the drifter properties as follows:

$$F_{drag} = 0.5 \cdot \rho \cdot C_d \cdot A_d \cdot v^2, \tag{3}$$

where ρ is the fluid density, C_d the drag coefficient, dependent on the shape of the body and the Reynolds number, A_d the projected surface area of the body perpendicular to the fluid flow and v the relative speed of the fluid compared to the drifter. Table II presents the lowest current drag force and highest wind drag force that occurred during the two test days. This shows that the wind drag is approximately 100 times smaller than the current drag and it was therefore neglected in the analysis. It should be noted that the drag coefficients of the sails and the floater were chosen based on their respective Reynolds and on their shape according to [16].

Similarly, one can compare the mass and the added mass of the drifter. The mass of one drifter was 5kg. The added mass of any drifter is related to its underwater volume, which was, in our case, composed of three parts: the submerged volume of the Styrofoam floater (V_F), the volume of the sails (V_S), and the volume of the poles holding the sails (V_P):

TABLE II
COMPARISON OF THE DRAG FORCES.

Parameter	Unit	Minimum F_{Dc} (current force)	Maximum F_{Dw} (wind force)
Re	-	6.10^5	1.10^5
ρ	kg/m^3	1000	1.3
C_d	-	2.0	1.1
A_d	m^2	0.592	0.045
V	m/s	0.25	3.5
F_{drag}	N	37	0.39

$$m_a = 0.5 \cdot \rho \cdot (V_F + V_S + V_P). \tag{4}$$

Given the high buoyancy of the floater and its geometry, its submerged volume was evaluated to be $4 \cdot 10^{-5} m^3$. The volume of the sails, corresponding to only thin plastic sheets, was completely neglected. The volume V_P, considering all poles as solids, was estimated to be $4.1 \cdot 10^{-4} m^3$. Using the density of the water, and Equation (4), this led to an added mass of $0.23kg$, which was 22 times smaller than the mass, and F_{m_a} was therefore be neglected.
The history force is more complex and describes the force due to the lagging boundary layer that occurs with variations of acceleration. This is a topic that has been well studied for spheres but not for cross

shapes. [17] shows that the history force causes inertial particles to stay closer to the flow and to behave more like tracers. Due to the complex nature of this force, it was not considered in this study. However, its possible impact will be discussed in the final section.
The pressure gradient force, in our context, is related to difference of pressure at the top of the sail and at the bottom of the sail. F_p would then lift up the bottom of the sail due to the additional pressure related to the additional water depth. However, the chain acted as a weight that countered that effect and kept the drifter vertical in the water. F_p was therefore neglected as well.

With all those considerations, Equation (2) can be simplified to

$$m \cdot \dot{v_d} = \begin{cases} -0.5 \cdot \rho \cdot C_d \cdot A_d \cdot (v_c - v_d)^2 & \text{if } \dot{v_d} < 0 \ , \\ +0.5 \cdot \rho \cdot C_d \cdot A_d \cdot (v_c - v_d)^2 & \text{if } \dot{v_d} > 0 \ , \end{cases} \quad (5)$$

where v_c is the current speed, v_d is the drifter speed, and $v_c - v_d$ corresponds to the flow speed as experienced by the drifter, which was simply noted v in the general Equation (3). Note that the two branches correspond to the cases where the drifter is decelerating and accelerating, respectively.

B. Current speed calculation

Equation (5) is equivalent to an equation with the form

$$K_1 \cdot v_c^2 - 2 \cdot K_1 \cdot v_d \cdot v_c + K_1 \cdot v_d^2 - m \cdot \dot{v_d} = 0, \quad (6)$$

in which

$$\begin{cases} K_1 = -0.5 \cdot \rho \cdot C_d \cdot A_d & \text{if } \dot{v_d} < 0 \ , \\ K_1 = 0.5 \cdot \rho \cdot C_d \cdot A_d & \text{if } \dot{v_d} > 0 \ . \end{cases} \quad (7)$$

Equation (6) is a quadratic equation with v_c as unknown that can easily be solved. The discriminant is

$$\delta = (2 \cdot K_1 \cdot v_d)^2 - 4 \cdot K_1 \cdot (K_1 \cdot v_d^2 - m \cdot \dot{v_d}), \quad (8)$$

which can be simplified to

$$\delta = 4 \cdot K_1 \cdot m \cdot \dot{v_d}. \quad (9)$$

Because K_1 and $\dot{v_d}$ have always the same sign, δ is always positive, and the equation has always one or two real solutions:

$$v_c = \begin{cases} \frac{2 \cdot K_1 \cdot v_d - \sqrt{\delta}}{2 \cdot K_1} = \frac{2 \cdot K_1 \cdot v_d - \sqrt{4 \cdot K_1 \cdot m \cdot \dot{v_d}}}{2 \cdot K_1}, \\ \frac{2 \cdot K_1 \cdot v_d + \sqrt{\delta}}{2 \cdot K_1} = \frac{2 \cdot K_1 \cdot v_d + \sqrt{4 \cdot K_1 \cdot m \cdot \dot{v_d}}}{2 \cdot K_1}. \end{cases} \quad (10)$$

The solution is chosen so that $\dot{v_d}$ and $v_c - v_d$ have the same sign. In the first case, the solution can be written as

$$v_c = v_d - \sqrt{\frac{m \cdot \dot{v_d}}{0.5 \cdot \rho \cdot C_d \cdot A_d}}. \quad (11)$$

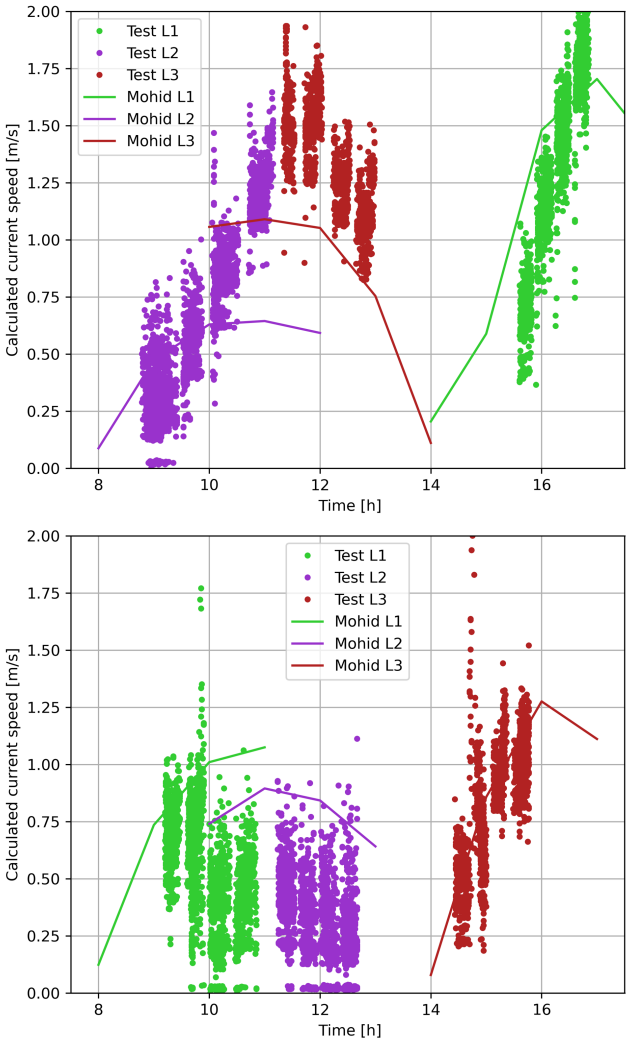

Fig. 12. Comparison of the measured current speed and MOHID's prediction. Top: Day 1. Bottom: Day 2.

C. Comparison with MOHID model results

Figure 12 presents the current speeds of all the points of all the tests and compares them with the current speed given by the operational model at the average location of all the launches for L1, L2 and L3, respectively. Figure 13 presents the same analysis, but corresponding to the direction of the current with a North facing orientation. It can be seen that the accelerating and decelerating trends of the current speed are well captured both in the experiment and in MOHID's results, but with some discrepancies in the accuracy of the value of the current speed. The changes in current directions corresponding to the changes of tides are also well represented despite a slight delay.

Figure 12 can however be misleading because all drifters were not released exactly at the same location, so variations between the results from MOHID model and the tests are expected. To facilitate a more relevant comparison, and given the difference of discretisation in time and space between the drifter test and the prediction from the Tagus estuary operational model, an interpolation was done on the outputs of the model. To do so, the average GPS location of each test was used to find the closest cell of the grid used by the

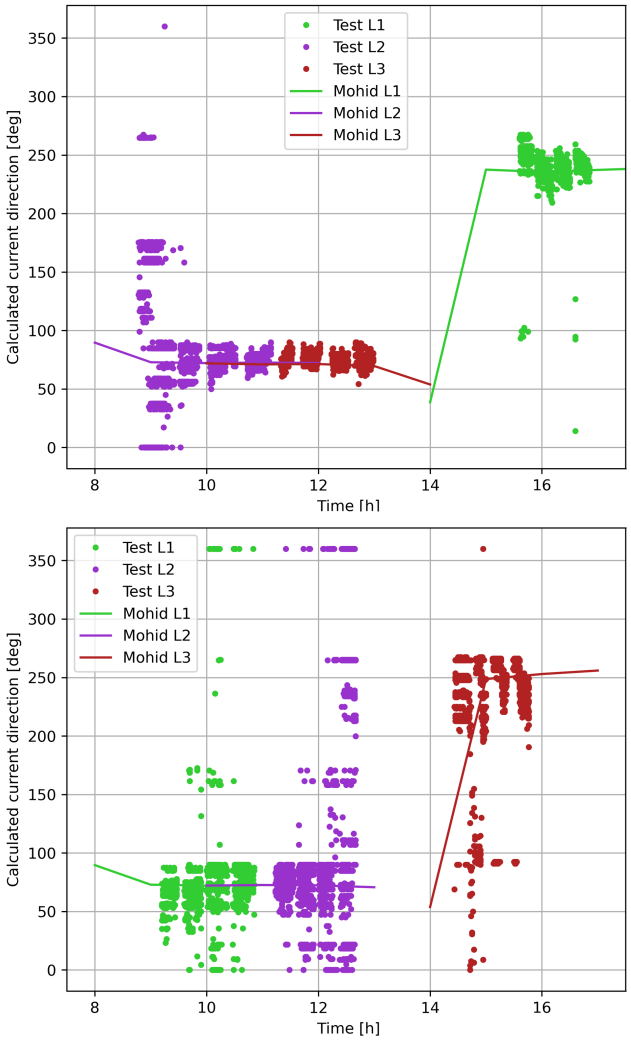

Fig. 13. Comparison of the measured current direction and MOHID's prediction.. Top: day 1. Bottom: day2.

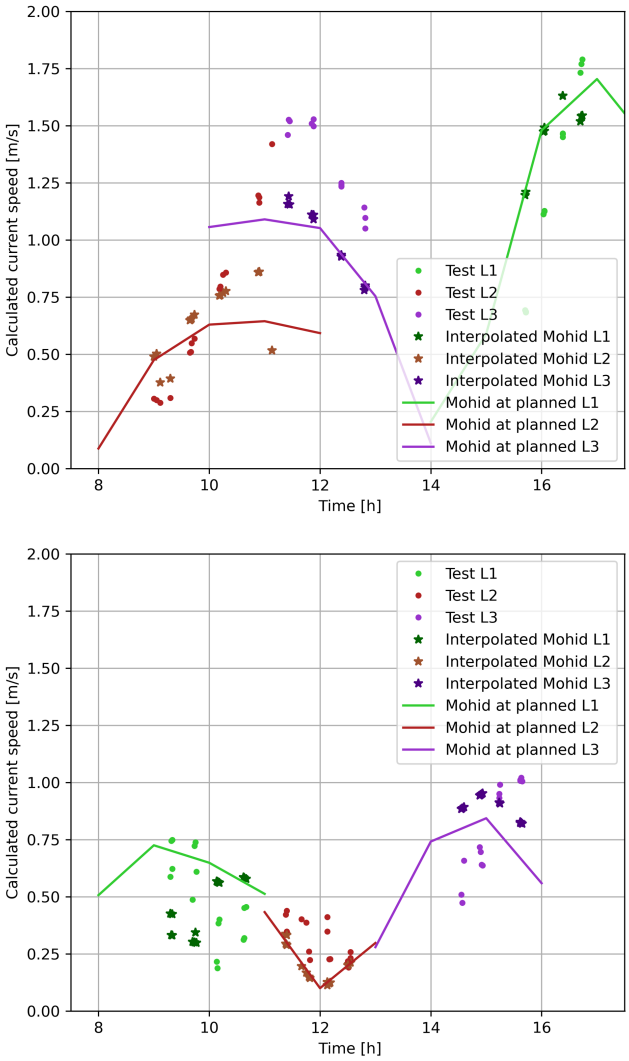

Fig. 14. Comparison of the measured current speed and MOHID's prediction. Top: Day 1. Bottom: Day 2.

operational model. Within this cell, a linear interpolation was used to approximate the current speed at any point in time between the hourly predictions of the model. This analysis is presented in Figure 14. Errors between the measured current speed and the interpolated numerical data, respectively the dots and stars in Figure 14, are still noticeable. Figure 15 presents this error for each tests. It shows that regardless of the test location, the test day, or the current speed, the error is constrained within 0.3m/s. The relative error can be quite high for low currents, but acceptable for the highest currents, which are, in any case, the most relevant for the evaluation of a tidal site. A discussion about the potential source of those errors is presented in Section VI.

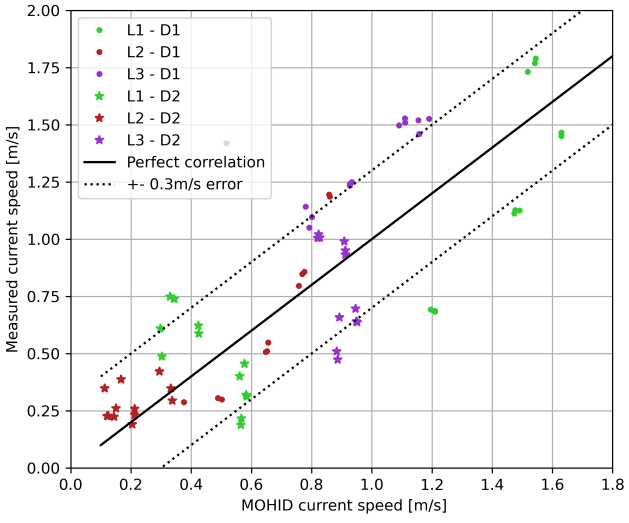

Fig. 15. Error between the measured current speed and MOHID's prediction.

VI. Discussion

A. Epistemic uncertainty of the experimental data

Given the Equation (11), errors in ρ, C_d and A_d should have a similar impact on the results: a positive error will decrease v_c. However, an increase in mass will increase v_c. It should also be noted that the percentage of error that those parameters have on v_c depends on v_d: the higher the drifter speed, the least impact ρ, C_d, m and A_d will have. Nonetheless, the impact of those parameters is minimal, even with a

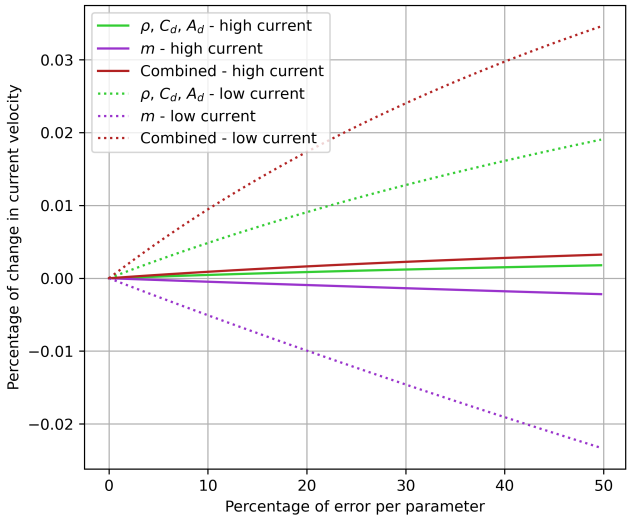

Fig. 16. Impact of input uncertainties on the current speed calculation.

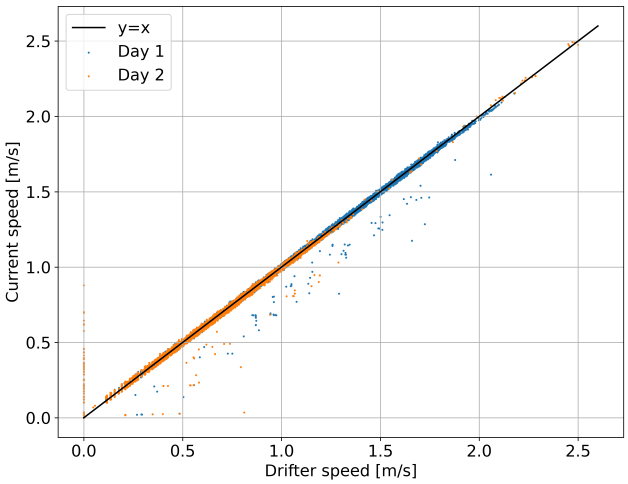

Fig. 17. Correlation between drifter and current speed.

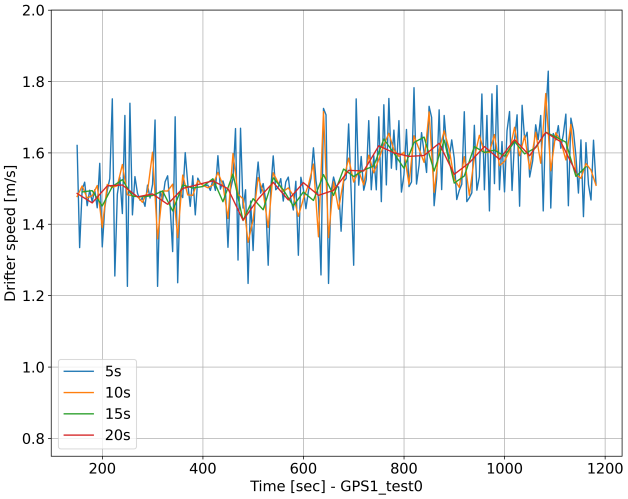

Fig. 18. Impact of time smoothing window on the drift speed assessment.

low v_d: given the low mass of drifter and its high drag force (due to the large dimension of the sails), the second term of Equation (11) can be considered as a corrective term with only a minimal impact on the current speed calculation. In fact, an error of 50% in mass will only introduce an error inferior to 0.1% in the final results, as presented in Figure 16, which shows the sensitivity analysis for the first test of day 1, during a low current speed, and the last test of day 1, during a high current speed. This shows that thanks to the design of the drifter, the current speed and the drifter speed are very similar. Figure 17 shows a scatter plots of v_c and v_d that highlights this result: the drifter speed is consistently very slightly above the current speed.

The main parameters to ensure the accuracy of the current measurement is in fact the accuracy of GPS, which should be adapted to the drifting speed. Indeed, as stated in Section III A, the GPS accuracy is 1m. This leads to an uncertainty of $\pm 2m$ in terms of travelled distance by the drifter between two measured points. Considering the time smoothing window of 5sec, this is equivalent to an uncertainty of $\pm 0.4m/s$ in the measurement of v_d. Increasing the time window could decrease that uncertainty. However the width of the window has very little impact on the average of the drifter's speed, as presented in Figure 18. Because of this limited impact and because some tests have few data points, the window was kept at 5 seconds, which allowed to maintain a consistent analysis throughout the study. In the future, a more accurate GPS or longer measurement periods should be used to prevent this issue.

B. Aleatory uncertainty of the experimental data

At each location, four drifters were released almost simultaneously, and each run was repeated four times. This enables the quantification of the aleatory character of each run. Table III presents the standard deviation of the current speed for all runs of 4 drifters and shows

TABLE III
ALEATORY UNCERTAINTY.

Test	Run1	Run2	Run3	Run4	Average
L1 D1	1%	1%	0%	1%	1%
L2 D1	3%	5%	4%	8%	5%
L3 D1	2%	1%	0%	3%	2%
L1 D2	11%	16%	32%	18%	19%
L2 D2	16%	24%	26%	11%	19%
L3 D2	17%	21%	3%	1%	10%

that uncertainties are much higher during the second day of testing. This can be related to the relative slow current speeds during that day. Indeed, the drag force induced by the tidal current becomes less predominant and the drifters can then be more sensitive to other effects that were not taken into account into the analysis, as detailed in section V A. This is also visible in 10, where the trajectories of the drifters are less directional on day 2 than on day 1.

C. Numerical discretisation of the Tagus estuary model

The time and spatial discretization of MOHID and of the experiment are significantly different: 1 hour against 1 second and 1m against 200m. Any turbulence that might affect the current speed at a small scale is therefore cut-off from model analysis. In addition, the horizontal discretization used in the model (200m) is also a limitation in the accuracy of the representation the river bed, and therefore in the accuracy of the description of the phenomena driving the flow. Those scale differences can explain the discrepancies between the experiment and the model. This assumption should be verified by running MOHID with a more refined mesh and a smaller time step. This is possible thanks to the nested model approach facilitated by the software structure, and will be the topic of another study.
The numerical discretisation of MOHID is not the only source of error. Indeed, as described in section V, multiple forces have been neglected. To correctly assess the influence of each of the forces, a complete hydrodynamic analysis of the drifter would be needed, including the effect of a turbulent and highly variable flow. However, one might argue that this complex analysis is not completely relevant for the comparison of potential tidal sites. Indeed this analysis would be cumbersome for potentially limited gains in the accuracy of the results, based on the discussion of forces acting on the drifter and the impact of certain parameters. In fact, the changes would be even smaller for the highest energetic sites, which are the most relevant for the selection of a location for tidal turbines.

VII. Conclusion

In this paper, we presented both a numerical analysis, using the numerical tool MOHID, and a low-cost experimental setup, using GPS-tracked drifters, to measure the current velocity in the Tagus Estuary in Portugal and to allow the selection of potential tidal energy sites from a hydrodynamic point of view. The method to derive the current speed from the drifter GPS logs was presented and the results were compared to the prediction proposed by the numerical tool. Despite a limited error in the current intensity up to $0.3m/s$, the trends of both approaches are similar, which justify the use of either approach for the comparison of the three sites. However, further analysis is needed to understand the discrepancies between the model and the experiments. In particular, the numerical analysis should be conducted again using results from a model with a higher resolution in time and space. In addition, it was shown that the critical parameter to decrease the uncertainty in current speed estimation is the GPS accuracy. GPS with a better accuracy in localisation should therefore be used, especially for sites with relatively low current speeds.

Acknowledgement

The authors would like to thank Sustainable Marine (https://www.sustainablemarine.com/) for sponsoring the purchase of the drifters. In addition, the authors thank the Câmara Municipal de Lisboa for providing access to the RIB used during the experiments. Finally, the Administraçao do Porto de Lisboa (https://www.portodelisboa.pt/) and the Capitania do Porto de Lisboa (https://www.amn.pt) are thanked for providing the necessary permits in short notice to account for the weather windows known only one day ahead.

References

[1] IEA, "Global Energy Review 2020," 2020. [Online]. Available: https://www.iea.org/reports/global-energy-review-2020
[2] I. da Conservação da Natureza e das Florestas, "Geologia, hidrologia e clima da Reserva Natural do Estuário do Tejo," 2022. [Online]. Available: http://www2.icnf.pt/portal/ap/r-nat/rnet/geo
[3] J. Rolim, "Modelação hidrodinâmica da sobreelevação do nível do mar de origem meteorológica no estuário do Tejo," Ph.D. dissertation, Instituto Superior Técnico, 2014.
[4] F. dos S. da S. Neves, "Dynamics and hydrology of the Tagus Estuary: results from 'in situ' observations," Ph.D. dissertation, Faculty of Science of the University of Lisbon, 2010. [Online]. Available: http://repositorio.ul.pt/handle/10451/2003
[5] Maretec, "MOHID - Water Modelling System." [Online]. Available: https://github.com/Mohid-Water-Modelling-System
[6] R. Neves, "A Bidimensional Model for Residual Circulation in Coastal Zones. Application to the Sado Estuary." *Annalles Geophysicae*, vol. 46, no. 3-4, pp. 465–472, 1985.
[7] F. Martins, "Modelação matemática tridimensional de escoamentos costeiros e estuarinos usando uma abordagem de coordenada vertical genérica," Ph.D. dissertation, Technical University of Lisbon, 1999. [Online]. Available: http://www.mohid.com/pages/home/whatismohid.shtml#ref_d
[8] H. dePablo, J. Sobrinho, M. Garcia, F. Campuzano, M. Juliano, and R. Neves, "Validation of the 3D-MOHID Hydrodynamic Model for the Tagus Coastal Area," *Water, Hydrology*, vol. 11, p. 1713, 2019.
[9] G. Franz, L. Pinto, I. Ascione, M. Mateus, R. Fernandes, and P. N. R. Leitão, "Modelling of cohesive sediment dynamics in tidal estuarine systems: Case study of Tagus estuary, Portugal," *Estuarine, Coastal and Shelf Science*, vol. 151, pp. 34–44, 2014.
[10] [Online]. Available: http://thredds.maretec.org/thredds/catalog/MOHID_WATER/TAGUSESTUARY_200M_1L_1H/FORECAST/catalog.html
[11] M. Mateus, G. Riflet, P. Chambel, L. Fernandes, R. Fernandes, M. Juliano, F. Campuzano, H. de Pablo, and R. Neves, "An operational model for the West Iberian coast: products and services," *Ocean Science*, no. 8, p. 713–732, 2012.
[12] F. Lyard, F. Lefevre, T. Letellier, and et al, "Modelling the global ocean tides: modern insights from FES2004," *Ocean Dynamics*, no. 59, p. 394–415, 2006.
[13] F. Judge, F. Devoy McAuliffe, I. Bakken Sperstaf, B. Chester R., Flannery, L. K., and J. Murphy, "A lifecycle financial analysis model for offshore wind farms," *Renewable and Sustainable Energy Reviews*, vol. 103, pp. 370–383, 2019.
[14] [Online]. Available: https://geopy.readthedocs.io/en/stable/#
[15] J. Kuerten, "Point-Particle DNS and LES of Particle-Laden Turbulent flow - a state-of-the-art review," *Flow Turbulence Combust*, 2016.
[16] S. Hoerner, "Fluid-dynamic drag theoretical, experimental and statistical information," 1965.
[17] A. Daitche, "On the role of the history force for inertial particles in turbulence," *Journal of Fluid Mechanics*, 2015.